journal of the mechanical behavior of biomedical materials 160 (2024) 106722

Contents lists available at ScienceDirect

Journal of the Mechanical Behavior of Biomedical Materials

journal homepage: www.elsevier.com/locate/jmbbm

Evidence of time dependent degradation of polypropylene surgical mesh explanted from the abdomen and vagina of sheep

Nicholas T.H. Farr [a,b,*], David A. Gregory [a,b], Victoria L. Workman [a,b], Cassandra Rauert [c], Sabiniano Roman [a], Alexander J. Knight [d], Anthony J. Bullock [a], Alexander I. Tartakovskii [d], Kevin V. Thomas [c], Christopher R. Chapple [e], Jan Deprest [f,g,h], Sheila MacNeil [a], Cornelia Rodenburg [a,b]

[a] School of Chemical, Materials and Biological Engineering, University of Sheffield, Sheffield, UK
[b] Insigneo Institute for in silico Medicine, University of Sheffield, Sheffield Teaching Hospitals NHS Foundation Trust, Sheffield Children's NHS Foundation Trust and Doncaster and Bassetlaw Teaching Hospitals NHS Foundation Trust, Sheffield, UK
[c] Queensland Alliance for Environmental Health Sciences (QAEHS), The University of Queensland, Woolloongabba, Australia
[d] Department of Physics and Astronomy, University of Sheffield, Sheffield, UK
[e] Department of Urology, Royal Hallamshire Hospital, Urology Clinic, Sheffield, UK
[f] Centre for Surgical Technologies, Group Biomedical Sciences, KU Leuven, Leuven, Belgium
[g] Department of Development and Regeneration, Woman and Child, Group Biomedical Sciences, KU Leuven, Leuven, Belgium
[h] Pelvic Floor Unit, University Hospitals KU Leuven, Leuven, Belgium

A B S T R A C T

The failure of polypropylene mesh is marked by significant side effects and debilitation, arising from a complex interplay of factors. One key contributor is the pronounced physico-mechanical mismatch between the polypropylene (PP) fibres and surrounding tissues, resulting in substantial physical damage, inflammation, and persistent pain. However, the primary cause of sustained inflammation due to polypropylene itself remains incompletely understood. This study comprises a comprehensive, multi-pronged investigation to unravel the effects of implantation on a presumed inert PP mesh in sheep. Employing both advanced and conventional techniques to discern the physical and chemical transformations of the implanted PP. Our analyses reveal a surface degradation and oxidation of polypropylene fibres after 60 days implantation, persisting and intensifying at the 180-day mark. The emergence and accumulation of PP debris in the tissue surrounding the implant also increased with implantation time. We demonstrate observable physical and mechanical alterations in the fibre surface and stiffness. Our study shows surface alterations which indicate that PP is evidently less chemically inert than was initially presumed. These findings underscore the need for a re-evaluation of the biocompatibility and long-term consequences of using PP mesh implants.

1. Introduction

Surgical mesh is often used to support tissues or strengthen repairs to soft tissues. A notable application of mesh is to support prolapsed organs, either temporarily or permanently. Surgical mesh made of polypropylene (PP) has been used since the 1950's to repair abdominal wall hernias such as incisional and inguinal hernias (Usher et al., 1958; Usher, 1962). Following initial modification of the mesh to reduce the observed host inflammatory response when used for abdominal hernia repair this use of the mesh was judged to be relatively successful with low recurrence rates being recorded (Kroese et al., 2017). Gynaecologists in the 1970's then started using PP meshes for pelvic organ prolapse (POP) interventions and then later for treatment of stress urinary incontinence (SUI) (Ulmsten et al., 1996). With the high prevalence of POP, 5–10 % (Milsom et al., 2014), PP surgical mesh was deployed routinely in women for many years.

Unfortunately, PP surgical mesh was not tested for suitability at the site of implantation rather an assumption was made based on the success of PP mesh used to treat abdominal hernias that the same mesh would work equally well in the pelvic floor. This assumption has proved to be incorrect as the use of PP surgical mesh for pelvic floor reconstructive surgeries has yielded complications in around 10 % of patients after vaginal insertion (Abed et al., 2011). Patients have suffered from sustained inflammation around the mesh, with contraction and even extrusion of mesh through patient's tissues (Mangir et al., 2019). There is now mounting evidence that PP may not be suitable for this purpose. This concern is shared by regulators who have now banned the use of PP mesh for most pelvic procedures in many countries including New

* Corresponding author. School of Chemical, Materials and Biological Engineering, University of Sheffield, Sheffield, UK.
E-mail address: n.t.farr@sheffield.ac.uk (N.T.H. Farr).

https://doi.org/10.1016/j.jmbbm.2024.106722
Received 9 May 2024; Received in revised form 26 August 2024; Accepted 3 September 2024
Available online 5 September 2024

Zealand, Australia, and the UK. The safety of remaining PP products has been called into question by health agencies in the USA and Canada.

Manufacturers have stated that PP surgical mesh is non-degradable in the body, but it has been hypothesised by many that the poor biostability of PP (especially when subject to repeated dynamic distension) is a key issue leading to surgical mesh complications (Imel et al., 2015; Iakovlev et al., 2017; Taylor, 2018; Talley et al., 2017; Clavé et al., 2010; Farr et al., 2021a; Jain et al., 2023; Farr et al., 2023a). We have provided *in vitro* evidence that PP mesh copes poorly with mechanical distension (Roman et al., 2019) and exposure to reactive oxygen species (ROS) as would be produced by inflammatory cells. Essentially it is strong but inflexible undergoing irreversible distension when subjected to repeated distension. Our previous studies have suggested degraded PP mesh has reduced bulk fibre tensile strength (Farr et al., 2021a; Roman et al., 2019) and undergoes an altered surface morphology as a consequence of interaction with immune cells (Farr et al., 2024).

Previous studies have recently examined PP surgical mesh explanted from animals and humans but the use of fixatives and storage procedures have cast some doubt on the validity of their findings (Thames et al., 2017). For these reasons the aim in this study is to produce the most comprehensive materials characterisation of explanted surgical mesh completed to date. Techniques applied in the study have been chosen not only to build on previous study results, but also to provide further data to support the proposal of new mechanisms by which PP surgical mesh degrades *in vivo*. This study presents for the first time the identification of PP debris within host tissues, cleaved from implanted surgical mesh *in vivo*. The application of novel imaging techniques has allowed us to visualise the interaction of PP surgical mesh with native tissues taken from a sheep model which was the first study to demonstrate that there are site specific differences in the response to PP mesh. We now provide detailed materials characterisation which gives us an important step forward in the understanding of PP based mesh interactions with tissues.

2. Materials and methods

A workflow of the experimental set up is presented in Fig. 1.

2.1. Materials

The samples characterised in this study were from the same tissue blocks as those described in Hympánová et al. (2020). All samples had been stored at −80 °C until required. In brief, polypropylene surgical mesh (Restorelle; Pore size 3.1 mm^2, Density g/m^2, supplied by Coloplast, Humlebaek, Denmark) was implanted into multiparous Lakens sheep (n = 24). Sheep were seven years old having had each more than four vaginal deliveries and weighing 51.5 ± 5.7 kg. Animals were housed week after surgery at the animal facility and then at the farm with unrestricted access to the food, water, chow and with free access to open space. Meshes were fixed with interrupted non-degradable 3/0 PP (Prolene, Ethicon, Zaventem, Belgium) sutures in the corners and halfway along each side. The mesh was implanted into either the rectovaginal septum or the abdomen. Although this model lacks the mechanical tension that mesh devices would experience in patients with prolapse it is the most relevant model currently available to assess integration and host response of the biomaterial within the relevant anatomical site. The material was explanted from sheep at two time points; 60 days or 180 days after implantation. To avoid the risk of damaging the mesh during explanation the tissues containing mesh were explanted and dissected into tissue blocks. The tissue blocks were then frozen and stored prior to analysis. This storage process avoided the use of any fixatives which could affect the surface of the mesh prior to characterisation. This experiment was approved by the Ethics Committee on Animal Experimentation of the Faculty of Medicine, KU Leuven, Belgium.

Fig. 2 presents images of explanted mesh with surrounding tissue after haematoxylin and eosin (H&E) or immunohistochemical staining. This data along with additional histology and immunohistochemistry is available in a previously published study (Hympánová et al., 2020) and is presented here for clarity to demonstrate the tissue blocks that were used in this follow-up study.

2.2. Identification of polypropylene particle debris within tissues

2.2.1. Pyrolysis gas chromatography mass spectrometry (Py-GC-MS)

Before analysis with Py-GC-MS could be performed, the tissue explanted from the abdomen and vagina from the two time points was digested to remove organic material. Tissue samples, including a sham control (containing explanted tissue with no mesh), were treated with an alkaline solution (pH 8.5–9.5) containing protease (Alcalase®, Merck, UK) at 37 °C for 72 h. The protease Alcalase® digests the tissue producing a hydrolysed tissue solution. Any visible surgical mesh fibres present were then carefully removed from the solution. The solution was then diluted with dH_20.

Polypropylene particles present in the incubation solutions were quantified using Py-GC-MS. First, any remaining tissue was removed from the samples by digesting with H_2O_2. Approximately 20 mL of H_2O_2 was slowly added to the sample, then the sample was incubated (Orbital Incubator shaker, Thermoline Scientific, Wetherill Park, NSW) at 60 °C for 48 h. The digest sample was then filtered through a 1.0 μm glass fibre filter (21 mm, GA-100, Stirlitech, WA, USA) and the filtrate filtered again through a 0.3 μm glass fibre filter (21 mm, GF-75, Stirlitech, WA, USA). This provided two size fractions of the captured particles, sizes >1.0 μm (microplastics) and sizes between 0.3 and 1.0 μm (nanoplastics). The filter papers were individually rolled and inserted into an 80 μL pyrolysis cup (Eco-Cup LF, Frontier Laboratories, Japan). The sample cups were then spiked with 40 μg of deuterated polystyrene (d5-PS, Polymer Source Inc., Dorval, Canada) as an internal standard. Samples were analysed with a multi-shot micro-furnace pyrolyzer (EGA/PY-3030D) coupled with a GC2030 GCMS (Shimadzu Corporation, Japan), using a double shot method and data was collected in full scan mode over a mass range of 40–600 m/z, following previously reported methodologies (Wang et al., 2021). The polypropylene pyrolysis product 2,4-dimethyl-1-heptene was monitored (m/z 126, 83, 70) to quantify the mass of polypropylene in each sample. The final concentrations were normalised to the initial amount of mesh from the sample.

Unfixed, frozen tissue samples were cut into sections 5 μm thick using a cryostat after being mounted in tissue freezing medium (Leica, UK). Brightfield images were taken using an upright compound microscope (Olympus CX43) and Euromex HD-Ultra camera (both supplied by Best Scientific, Wiltshire, UK).

2.2.2. Nano-Fourier transform infrared spectroscopy (nano-FTIR); scattering-type, scanning near-field optical microscopy (s-SNOM)

Standard optical microscopy techniques were first applied to identify regions containing polypropylene particles as areas exhibiting strong light scattering behaviour. However, these techniques were unable to characterise these regions in detail. s-SNOM was able to distinguish between the polymer mesh and the surrounding organic tissue due to the large difference in refractive index between the polypropylene particles and the sheep tissue at the measured wavelength (1370 cm^{-1}).

AFM, s-SNOM, and Nano-FTIR data were all collected under ambient conditions utilising a neaSCOPE from Attocube Systems AG/Neaspec.

AFM Data: AFM topology information was collected using a neaSCOPE system, and a conductive Pt/Ir cantilever (ARROW-EFM from Nanoworld) to allow for the simultaneous collection of s-SNOM data. A tapping amplitude and frequency of 87 nm and 80 kHz were used.

s-SNOM: 1370 cm^{-1} light from a single-wavelength tuneable source (MIRcat-QT from Daylight Solutions) was sent into a Michaelson interferometer. One arm of the interferometer hosted an AFM employing a conductive cantilever to measure the sample in tapping mode (tapping frequency 80–82 kHz, tapping amplitude 60–87 nm). The incident light was focused onto the tip of the AFM cantilever and interacted with the

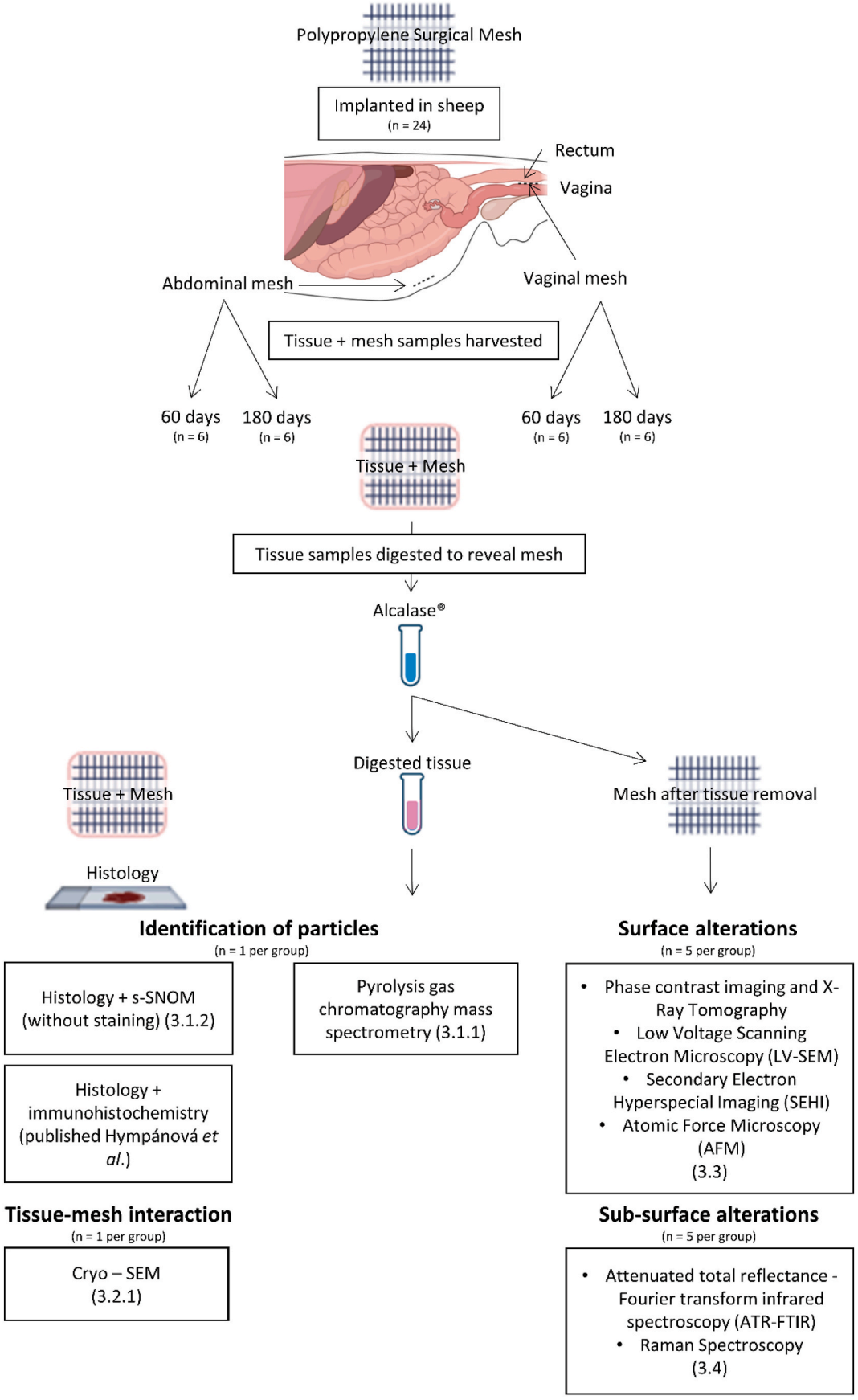

Fig. 1. Workflow of the experimental set up. Section numbers for the relevant results are in brackets.

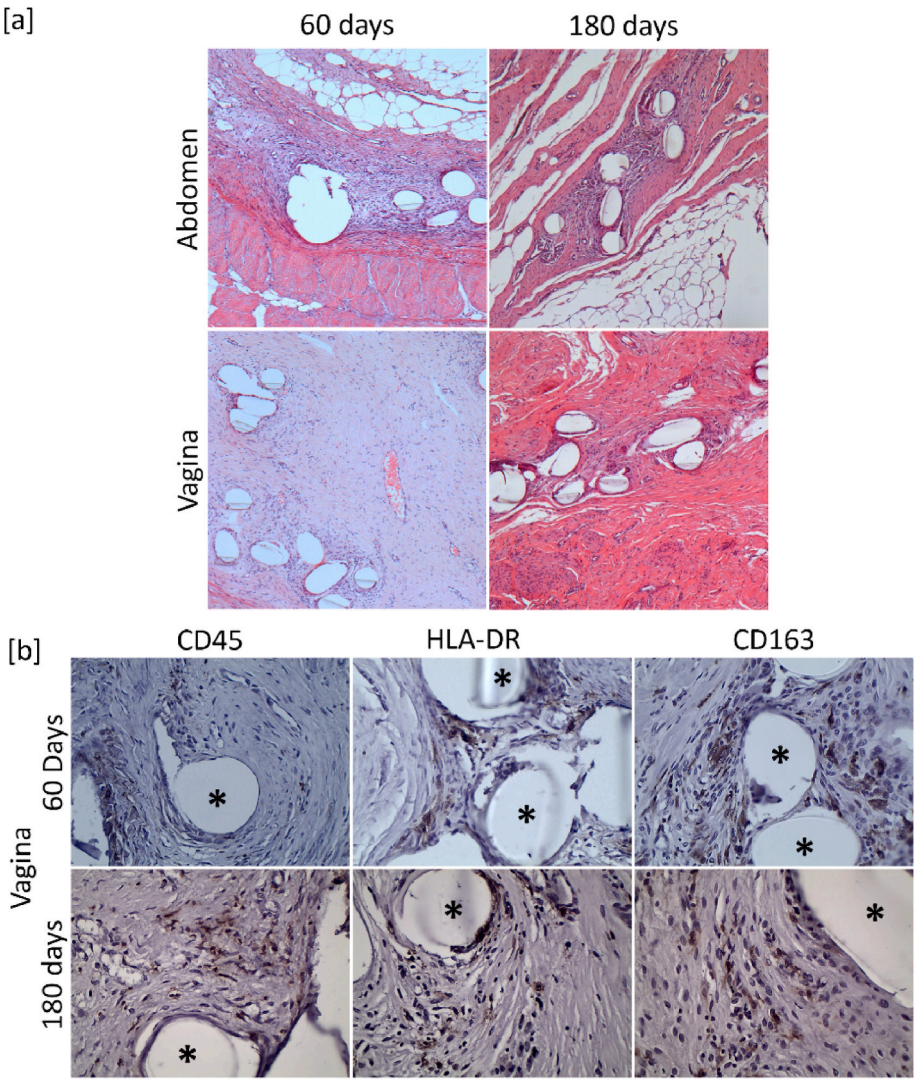

Fig. 2. Histology images of explanted mesh and surrounding tissue. [a] Haematoxylin and eosin stained samples of mesh and tissue explanted from abdomen and vagina at 60 and 180 days. 10× magnification. [b] Immunohistochemical staining of mesh and explanted tissue from vagina at 60 and 180 days for leukocytes (CD45), macrophage type 1 (HLA-DR), and macrophage type 2 (CD163). 40× magnification. Mesh structures are represented by asterisks. CD = cluster of differentiation; HLA-DR = human leukocyte antigen–antigen D related.

tip-sample system to generate a near-field probe of the sample. Scattered light from this system was collected back along the arm of the interferometer. The second arm of the interferometer hosted a moveable mirror that was dithered to generate a modulation in an otherwise clean reference signal. Both the signal and reference beams were recombined and interfered with each other at the detector. The overall signal was demodulated at a combination of the fourth harmonic of the AFM tapping frequency and the reference mirror dithering frequency to effectively remove the background scattering from the data. The complex data recorded was separated into an amplitude and phase component, with the amplitude data normalised to its maximum value, and the phase data normalised to a measurement of plain silicon made immediately after the sample measurement. A simple outlier filter was used to replace any especially low-signal data pixels with an average of the surrounding data pixels.

Nano-FTIR: The same system as described for the s-SNOM measurements was employed for nano-FTIR measurements, except that the single-wavelength light source was replaced with a broadband light source (FemtoFiber dichro midIR from TOPTICA Photonics), and the dithering mirror was replaced with a moveable mirror on a linear stage. AFM tapping parameters 80 nm amplitude and 80 kHz frequency were used. By moving the reference mirror along the linear stage (600 μm at a speed of 15 μm s^{-1}) an interferogram was obtained that could be converted into the spectra of the material's optical response via a Fourier transform. A reference measurement of plain silicon (made immediately after the sample scans) was used to reference the data, and a constant offset and linear gradient were subtracted from the data to account for thermal drift in the interferometer arms. 10 repeat scans were done for each measurement point and averaged over.

2.3. Assessment of polypropylene surgical mesh when in contact with native tissue

2.3.1. Cryo-low voltage (LV)-Scanning electron microscopy imaging

Cyro-scanning electron microscopy (Cryo-SEM) was conducted using the Quorum PP3010T cryo-SEM preparation system (Quorum Technologies Ltd., Laughton, East Sussex, UK). Specimens were mounted on a cryo-SEM shuttle, and plunge-frozen in slushed liquid nitrogen. The shuttle was then transferred to a cooled prep stage (−160 °C) before being loaded onto the cryo-stage (−160 °C) housed within the SEM chamber for imaging. An anti-contaminator was also placed within the chamber at a temperature of −185 °C.

A FEI Helios Nanolab G3 (FEI Company, US) microscope was employed for surface morphology observations of mesh samples. In contrast to common scanning electron microscopy (SEM) analysis practice, samples were not pre-treated with a conductive coating by deposition. An accelerating voltage of 1–2 keV at typical chamber vacuum pressures in the range of 10^{-6} mbar and a working distance of 4 mm were chosen to avoid sample damage through surface charging. An Everhart-Thornley Detector (ETD) was selected for low magnification of SE images and a Through Lens Detector (TLD) for high magnification SE images.

2.4. Assessment of polypropylene surface properties

Prior to materials characterisation, the explanted mesh samples were thoroughly cleaned by a previously established cleaning process to remove any biological tissue adhering to the mesh surface (Wang et al., 2021). Briefly, samples were treated with an alkaline solution (pH 8.5–9.5) containing protease (Alcalase®, Merck, UK) at 58 °C for 12 h. Common salt, tenside SUPRALAN UF (Zschimmer & Schwarz, Germany) and sodium carbonate were added to the solution to regulate the pH value. The protease Alcalase® is a serine endopeptidase primarily composed of subtilisin A, which is suitable for the hydrolysis of proteins and harmless to synthetic mesh materials. In other words, the cleaning process does not affect the mesh fibers (Wang et al., 2021). To further validate the use of Alcalase® and as a control for this study, non-implanted Restorelle mesh was treated with Alcalase® following the same process used for the tested materials. SEM, AFM, and ATR-FTIR analyses were performed, along with comparisons to previously published SEM images and ATR-FTIR spectra of control PP without Alcalase® treatment. These results are provided in the supporting information (Fig. SI 2).

2.4.1. Phase contrast imaging and X-Ray Tomography

In-line phase contrast imaging and tomography was performed on the Diamond Manchester Imaging Branchline at the Diamond Light Source, UK. A micro-imaging set up for samples with 0.1–10 mm thickness was selected and samples were imaged with spatial resolutions which extended a little above a micron. The high flux of a synchrotron enabled images of high signal:noise to be recorded very quickly. X-rays were converted to visible light by the scintillator; the visible light was then magnified and collected by a detector. A condenser lens known as a Fresnel zone plate focused the incoming light onto the sample. The light was then collected by a second zone plate (the objective lens) and a magnified image of the sample was projected onto the scintillator. For all materials a 0– 180-degree scan was applied with a 0.006 step size and 0.5 s exposure. 10× objective was selected for all of the measurements. This resulted in a field of view of 0.83 × 0.70 mm (horizontal x vertical) with 0.325 μm pixel size. After 3D reconstruction was completed with an in-house MATLAB package, 3D image analysis was performed using Avizo Software (Thermo Fisher Scientific).

2.4.2. Energy Dispersive X-ray spectroscopy

FEI Helios Nanolab G3 (FEI Company, USA) SEM equipped with an Energy Dispersive X-ray Spectroscopy (EDX) detector (Oxford Instruments, UK) was used to capture EDX. EDX spectra were obtained with a 10 keV accelerating voltage using a 13 nA probe current at a working distance of 5 mm. Data analysis was automated by the application of Aztec EDX analysis software (Oxford Instruments, UK).

2.4.3. Secondary electron hyperspectral imaging (SEHI)

In previous studies, the process of SEHI data acquisition has been described in great detail (Farr et al., 2021b; Nohl et al., 2022). Briefly, SEHI generation in this study was performed using a Helios Nanolab G3 microscope by applying consistent operating conditions of 1 keV and 50 pA immersion mode. This microscope can provide ultrahigh resolution images at voltages <1 keV. To ensure that images were taken of the true material surface, no conductive coating was applied to the samples in contrast to typical SEM analysis practice. At the time of analysis, a typical vacuum pressure of ~10^{-6} mbar was maintained at a working distance of 4 mm. The collection of SEHI of different energy ranges was enabled through the adjustment of the mirror electrode voltage (MV) together with a tube bias setting of 150 V. Stepping the MV in a range of −15 to 15 V was achieved through the use of an automatic iFast collection recipe. Every image was acquired at a frame interval of 0.5 s and an MV step size of 0.5 V, corresponding to an electron energy step size of about 0.2 eV. Image processing was done with Fiji ImageJ software (ImageJ, NIH USA).

2.4.4. Atomic force microscopy

Atomic force microscopy (AFM) microscopy was performed in tapping mode with SCANASYST-AIR probes under ambient conditions on a Bruker Dimension Icon AFM. Explanted mesh samples were placed on a cover glass and then attached to a magnetic AFMsupport. Different areas of the samples were analysed to produce peak force images obtained through PeakForce Tapping AFM mode, where the maximum value of the tip-surface interaction force is used as a constant setpoint for each pixel of the area scanned (Fakhrullina et al., 2017). Data analysis was performed using Brucker's NanoScope Analysis software (Version 2.0).

2.5. Quantification of Sub-surface chemistry

2.5.1. Attenuated total reflectance - Fourier-transform infrared spectroscopy

Infrared spectra were obtained for all test mesh samples with a NICOLET 380 Fourier-transform infrared (ATR-FTIR) spectrometer (ThermoFisher Scientific, US). Samples were purged with dry air before spectra collection in the range from 500 to 4000 cm^{-1} averaging 32 scans and a resolution of 4 cm^{-1}. The samples were analysed in their solid state form using an attenuated total reflection (ATR) accessory with a Golden Gate® diamond crystal (Specac, UK).

2.5.2. Raman spectroscopy

Raman spectroscopy (Renishaw inVia micro-Raman) was employed to analyse the chemical structure of explanted mesh samples. Raman spectra were collected from longitudinal fibres located distal to mesh knot sites. A 50× objective was selected with 10 s exposure. The laser power was set at 3 mW with a 1 μm spot size. A Peltier-cooled multichannel CCD detector was used for data recording with a 2400 lines/mm diffraction grating at a slit opening of 65 μm and a spectral resolution in the order of 1 cm^{-1}. For data analysis no smoothing was applied with baseline subtraction performed using OriginLab software (OriginLab Corporation, USA).

2.6. Statistical analysis

Statistical analysis and graph production was performed using GraphPad Prism version 9 software (GraphPad Software, Inc.; La Jolla, USA). Data are reported as mean±standard deviation. Sample numbers are provided in the experimental set up presented in Fig. 1. The significance level was defined as $p < 0.05$. For nonparametric analysis, the Mann–Whitney test was used for data that was not normally distributed.

3. Results

3.1. Identification of polypropylene particle debris within tissues

3.1.1. Pyrolysis gas chromatography mass spectrometry

Pyrolysis gas chromatography mass spectrometry was performed to identify if the presence of any PP debris could be detected within tissues surrounding explanted PP mesh. Polypropylene was detected in all digested tissue solutions at levels above that of the sham control (tissue only) (Fig. 3) with the majority of captured particles greater than 1 μm in

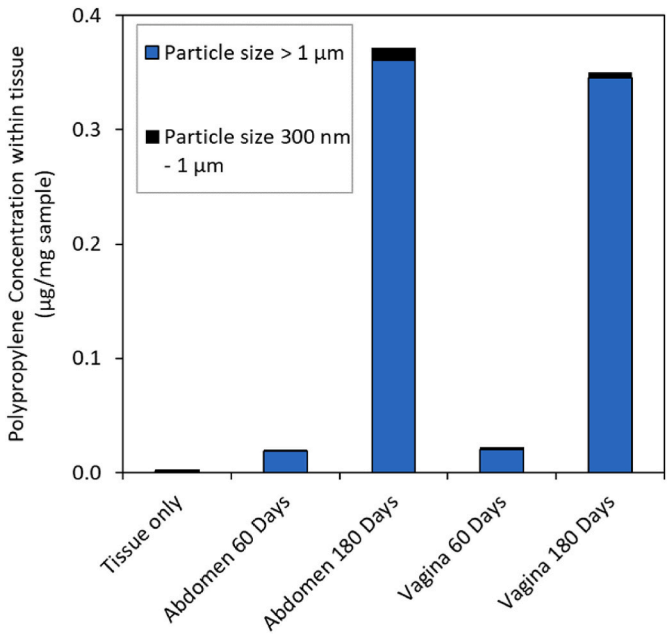

Fig. 3. Pyrolysis gas chromatography mass spectrometry of explanted tissues surrounding explanted polypropylene mesh (n = 1 for each explanted tissue site).

size. Solutions obtained from tissue explanted from the abdomen and vagina after 180 days contained notably more polypropylene debris than those of 60 days solutions.

3.1.2. Conventional histology and nano-Fourier transform infrared spectroscopy (nano-FTIR); scattering-type, scanning near-field optical microscopy (s-SNOM)

Following the observation of polypropylene particles being present in digested tissue solutions, s-SNOM and EDX (presented in Fig. SI 1) were performed in order to better visualise the polypropylene particles on prepared histology slides. The results presented in Fig. 4 show that the polypropylene particles are buried within the sheep tissue, vary markedly in size, and present strongly oxidised surface chemistry. An s-SNOM illumination wavelength of 1370 cm^{-1} was selected to correspond with the stretching absorption of the alkyl bonds (C-H) present in polypropylene. This wavelength has previously been used to normalise FTIR spectra for polypropylene (Jain et al., 2023). A scan area was selected by identifying an area of interest via optical microscopy. The s-SNOM scan results alongside AFM data are presented in Fig. 4a–c.

The AFM topology scan shown in Fig. 4a highlights that the polypropylene particles found in the sheep tissue were either partially or entirely embedded in the surface of the sample and are therefore difficult to identify via the topology data alone. SI Figure (Fig. SI 2) further highlights the embedded nature of the polypropylene particles by presenting the same data as in Fig. 4a and b in a 3D plot.

The s-SNOM scan data in Fig. 4b highlights the optical response from the polypropylene particles is stronger than the response from the sheep tissue due to the difference in refractive index between these materials at the measured wavelength (1370 cm^{-1}), allowing the polypropylene particles to be easily identified as areas of high s-SNOM amplitude signal, even when buried under a thin layer of tissue. The phase data in Fig. 4c highlights that there is some absorption at this wavelength from the polypropylene, in line with the result of (Farr et al., 2023b). Significant variation in particle size is observed in Fig. 4b.

In order to further investigate the surface chemistry of the polypropylene particles, nano-FTIR was performed on areas of the s-SNOM scan (Fig. 4b) highlighted with coloured circles. The nano-FTIR data from the polypropylene region (Fig. 4d) shows a broad absorption peak from around 1240–1460 wavenumbers, supporting the absorption at 1370 cm^{-1} observed in Fig. 4c on the polypropylene. Another, narrower peak is highlighted at 1740 cm^{-1} wavenumbers, which is attributed to C=O stretch vibrations (Imel et al., 2015; Farr et al., 2023a; Deplaine et al., 2013), suggesting that the surface of the polypropylene particles is highly oxidised. Fig. 4e presents the nano-FTIR data taken from the tissue area marked with a blue circle in Fig. 4b. The lack of significant feature overlap between the nano-FTIR scans in Fig. 4d and Fig. 4e highlight the very different optical nature of the two materials. Both nano-FTIR spectra were referenced to a silicon measurement made immediately after the sample scans. s-SNOM scans were also performed at 1370 cm^{-1} on other tissue samples, presented in Fig. 4f–h. In summary these analyses show evidence of time dependent generation of PP particles of around 1 µm which are oxidised occurring in both the abdomen and pelvic floor.

3.2. Assessment of polypropylene surgical mesh when in contact with native tissue

3.2.1. Cryo-low voltage (LV)-Scanning electron microscopy imaging

Cryo-LVSEM was preformed to image the surface morphology and tissue adhesion of the polypropylene surgical mesh for all sample groups (Fig. 5). All groups showed surgical mesh and tissue integration with what appears to be a protein deposition identifiable after 60 days of implantation. Imaging of all samples also revealed notable surface markings on the mesh fibres. Unlike fabrication markings, which run longitudinally, surface cracking was apparent running horizontally across the fibres. These cracks were more pronounced for both abdominal (Fig. 5a–d) and vaginal (Fig. 5e–h) implanted mesh over a 180-day period (Fig. 5 c–d, g-h) than observed over the shorter 60-day period (Fig. 5 a–b, e-f).

3.3. Assessment of polypropylene surface properties

3.3.1. X-Ray Tomography

After the removal of tissue using Alcalase® digestion solution, the surgical mesh samples from all groups were imaged using X-Ray Tomography at the UK Diamond Light Source. The rationale for removing the tissue was to ensure that the surface cracking observed on the mesh using Cryo-SEM was indeed a reflection of the true surface of the PP mesh, rather than structures from tissue/protein attachment. X-Ray Tomography provides a significant advantage in this study by allowing us to visualise the overall 3D structure of the mesh and the distribution of surface particles in a non-destructive manner. This method offers complementary data to the Cryo-SEM by enabling us to observe the surface features of the mesh in three dimensions, enhancing our understanding of the surface alterations and particle distribution over time.

The resultant 3D reconstructions are shown in Fig. 6. Notably, X-Ray Tomography reveals the presence of particles on the surface of all groups, consistent with the observations from Cryo-SEM. These particles are most prominent around knots and mesh friction sites, where mesh fibres can rub together during loading. However, they are also present along longitudinal fibres where no other mesh fibres are nearby. More surface particles are observed in the samples explanted after 180 days (Fig. 6 c–d, d-h) than in those explanted after 60 days (Fig. 6 a–b, e-f). Additionally, more pronounced surface alterations are observed in PP mesh explanted from the vagina (Fig. 6e–h) compared to that from the abdomen (Fig. 6a–d).

3.3.2. Low voltage (LV)-Scanning electron microscopy imaging and secondary electron hyperspectral imaging (SEHI)

In order to evaluate the surface morphology of the four explanted meshes, a series of SEM images were acquired (a methodology recommended by ISO 10993-18). The analysis was performed on uncoated mesh samples after the surrounding tissue was digested away. To

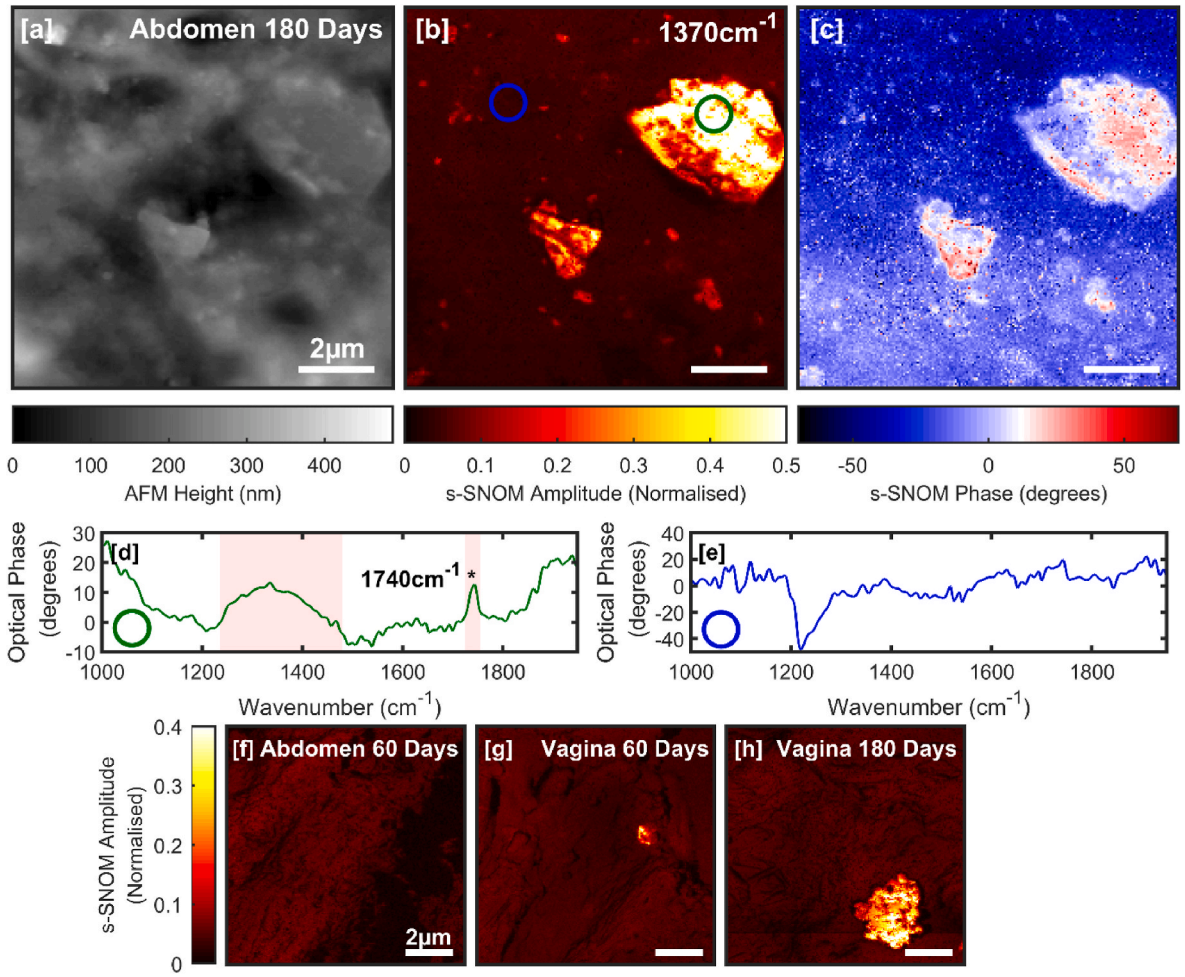

Fig. 4. AFM and near-field optical analysis of histology samples. [a] AFM topology scan of sheep abdomen tissue harvested 180 days after surgical implantation. This region of tissue was identified by optical microscopy as containing polypropylene particles. [b], [c] s-SNOM amplitude and phase data respectively, taken simultaneously with the AFM scan in [a], with an illumination frequency of 1370 cm^{-1}. Due to the difference in optical properties of the polypropylene and sheep tissue, a contrast in optical data is evident. s-SNOM amplitude data in [b] is normalised to the maximum recorded value of the scan, and the phase data in [c] is referenced to a silicon measurement made immediately after the tissue scan. Data in [b] and [c] have been smoothed with a simple outlier filter. [d], [e] Nano-FTIR data taken from a polypropylene particle (green circle in [b]) and tissue area (blue circle in [b]) respectively. Absorption peaks at around 1370 cm^{-1} and 1740 cm^{-1} in [d] are discussed in the main text. Nano-FTIR data were levelled, offset and normalised to a silicon measurement made immediately afterwards in order to account for thermal fluctuations, system response, and other error sources. [f], [g], [h]: Further s-SNOM amplitude scans at 1370 cm^{-1} taken from histology samples of: abdomen sheep tissue 60 days after implantation; vagina sheep tissue 60 days after implantation; vagina sheep tissue 180 days after implantation, respectively. Areas were first identified as containing polypropylene through optical microscopy, except for the area in [f] for which no polypropylene could be found. Data has been normalised and filtered similarly to that shown in [b].

mitigate the impact of sample charging and to generate highly surface sensitive images low voltage (LV)-SEM (1–2 keV) imaging was employed. LV-SEM images collected from the control mesh (treated with the protease Alcalase®) are presented in Fig. 7 a-b for comparison with the explanted mesh samples.

From the images presented, it is apparent that both environmental stress cracking (ESC) and surface degradation has occurred on all explanted PP meshes. It is also notable that this is more prominent for meshes which were implanted for longer, 180 days abdomen (Fig. 7e) and vagina (Fig. 7f) compared to those of 60 days abdomen (Fig. 7c) and vagina (Fig. 7d). For 180-day samples it is also notable that "barking" was observed. Barking, as shown in Fig. 7e–i, is a visible sign of surface degradation which has been observed in various other studies evaluating explanted PP meshes.

From all explanted meshes (n = 5) imaged, it was observed that the 180-day vagina mesh samples appeared to display the most extensive ESC both in terms of barking (Fig. 7g) but also in relation to observable horizontal cracking. To evaluate the surface chemistry of the 180-day vagina mesh samples SEHI was applied (Fig. 7h). SEHI has previously been applied to surgical mesh and its peak and chemical mapping abilities have been extensively published (Farr et al., 2021b; Nohl et al., 2022). In this study SEHI was applied to RGB mapping, corresponding to broad energy ranges relating to Red 0–2 eV (C-C), Green 2–4 eV (CH vibrations) and Blue 4–6 eV (C-O). From the SEHI map provided (Fig. 7h) the surface chemistry of the 180-day vagina mesh sample is not homogenous. Of particular interest is that where ESC cracks are observable there is a strong green (CH) emission. This indicates that the cracks are uncovering fresh regions of PP as the CH emission obtained is representative of the CH_3 methyl group present in PP.

3.3.3. *Atomic force microscopy (AFM)*

To investigate the surface roughness and stiffness of explanted PP mesh (after tissue digestion) AFM was performed. Fig. 8 presents 3D height maps, surface roughness values and 2D Young's Modulus scans of PP mesh explanted from both the abdomen (Fig. 8a–b) and vagina (Fig. 8c–d) after 60 (Fig. 8a and c) and 180 days (Fig. 8b and d). Two surface roughness parameters are provided: the roughness arithmetic average, often denoted as (Ra), is a parameter used to quantify the

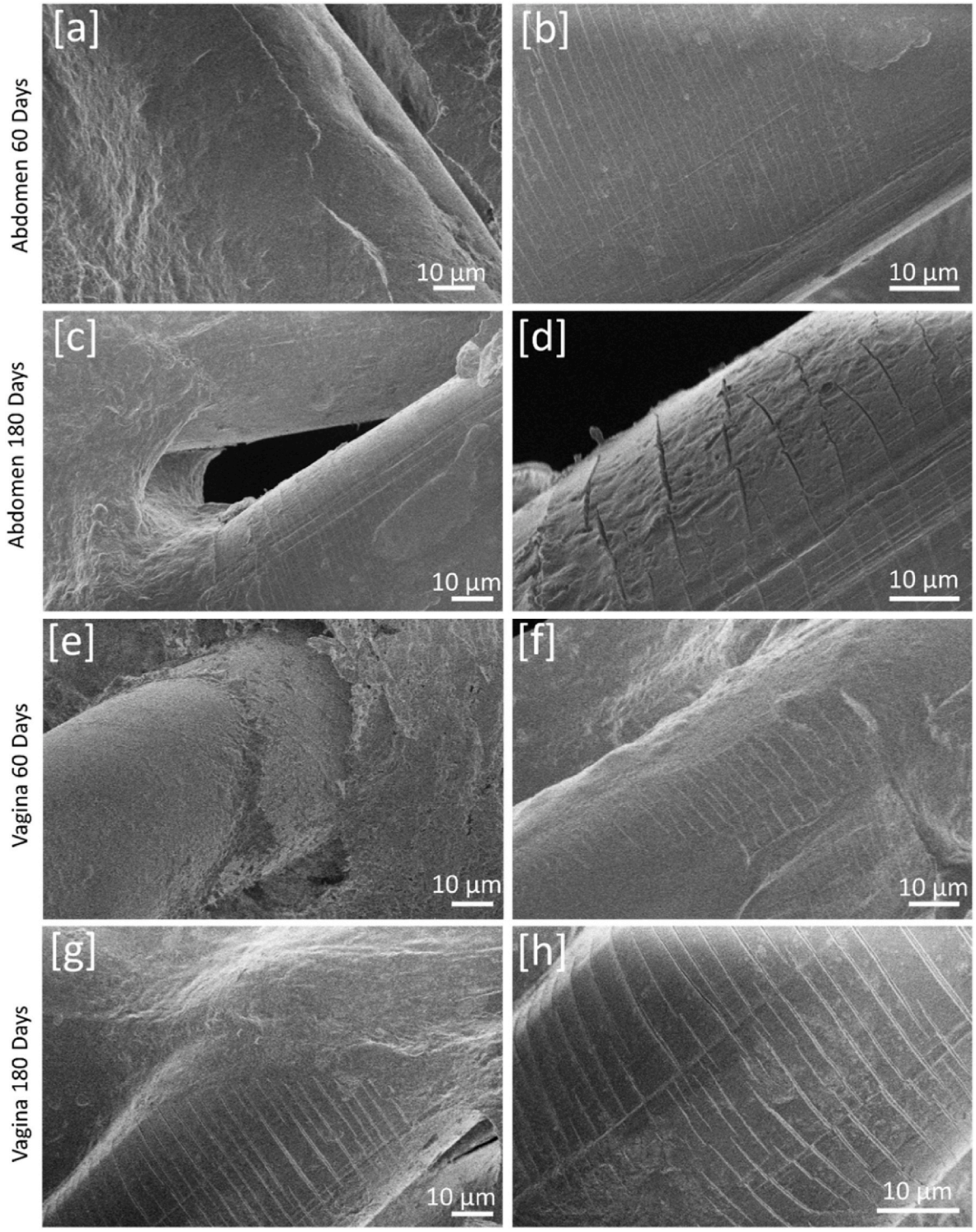

Fig. 5. Low-voltage scanning electron microscopy (LV-SEM) images captured under cryo-SEM conditions of explanted PP surgical mesh with attached native sheep tissue. [a-b] PP surgical mesh after 60-day implantation in a sheep abdomen. [c-d] PP surgical mesh after 180-day implantation in a sheep abdomen. [e-f] PP surgical mesh after 60-day implantation in a sheep vagina. [g-h] PP surgical mesh after 180-day implantation in a sheep vagina.

average roughness of a surface, while root mean square roughness (Rq) is meaningful in describing the surface roughness as it represents the standard deviation of the surface height distribution. For both implantation sites it is notable that the height variation (roughness) and Young's Modulus (surface stiffness) were greater after 180-day implantation compared to that of 60 days. Additionally, for both 60 and 180 day time points the implantation site also presented differences. Samples implanted for 60 and 180 days in the vagina exhibited greater surface roughness and stiffer surface regions than mesh explanted from the abdomen after 60 and 180 days.

Fig. 9a and b presents the distribution histograms of the Young's modulus obtained for explanted and control samples. As exhibited in Fig. 9, the Young's modulus for both abdomen (Fig. 9a) and vaginal samples (Fig. 9b) increases with the greater time of material

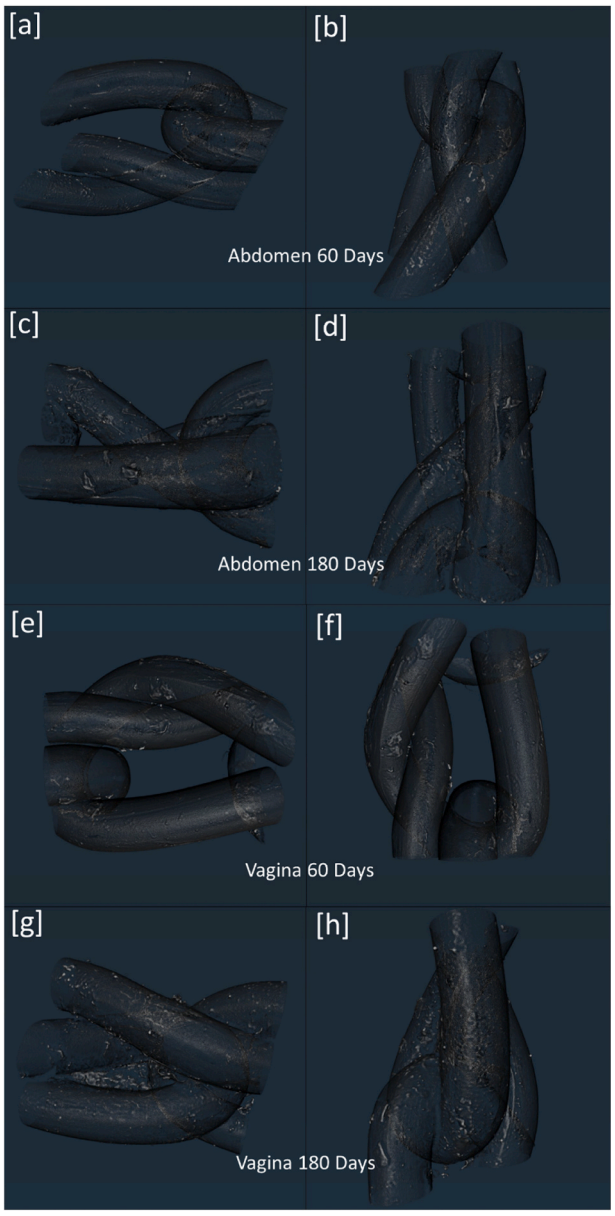

Fig. 6. Collection of X-Ray tomography 3D reconstructions of explanted PP surgical mesh after tissue digestion. [a-b] PP surgical mesh after 60-day implantation in a sheep abdomen. [c-d] PP surgical mesh after 180-day implantation in a sheep abdomen. [e-f] PP surgical mesh after 60-day implantation in a sheep vagina. [g-h] PP surgical mesh after 180-day implantation in a sheep vagina.

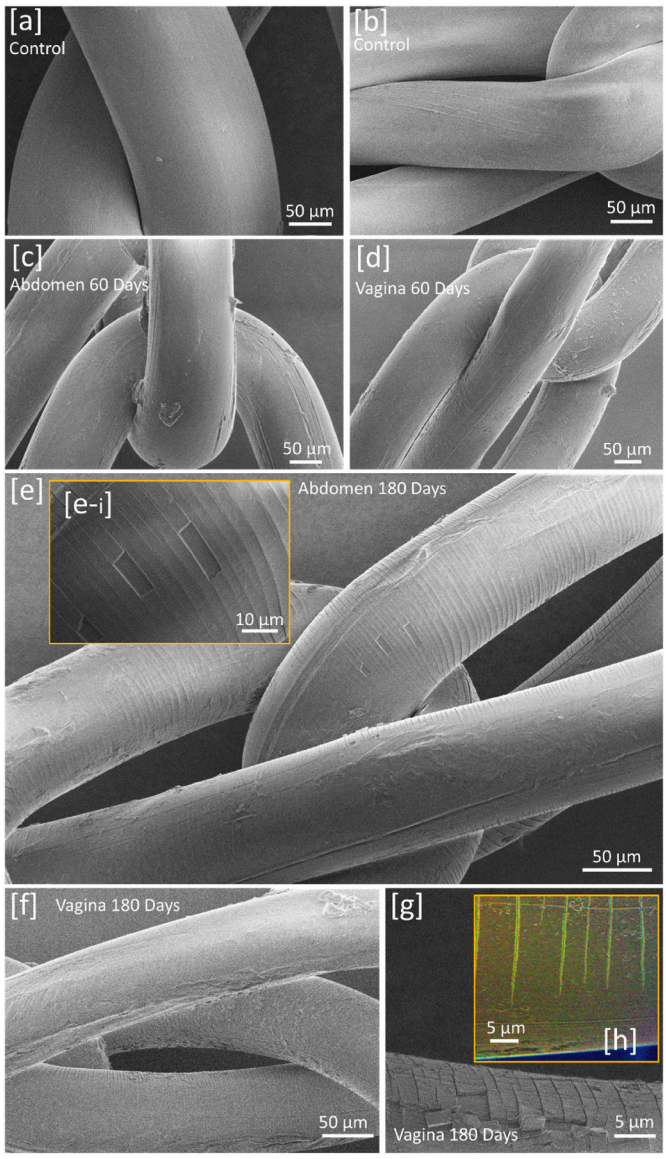

Fig. 7. Collection of low-voltage scanning electron microscopy (LV-SEM) images of explanted PP surgical mesh after tissue digestion. [a-b] Control non-implanted PP mesh. [c] PP surgical mesh after 60-day implantation in a sheep abdomen. [d] PP surgical mesh after 60-day implantation in a sheep vagina. [e] PP surgical mesh after 180-day implantation in a sheep abdomen. Inset [e-i] high resolution image of surface cracking. [f and g] PP surgical mesh after 180-day implantation in a sheep vagina. Inset [h] Secondary Electron Hyperspectral Image (SEHI) scan of PP surgical mesh after 180-day implantation in a sheep vagina.

implantation demonstrating a stiffening with time of implantation (Fig. 9d). It is also notable that samples taken from the vagina show an increase in the variance in their Young's modulus compared to that of the abdomen (Fig. 9c).

3.4. Quantification of Sub-surface chemistry

To obtain a measure of the bulk oxidation, ATR-FTIR was performed. ATR-FTIR is recommended for determining the chemical structure of synthetic polymers used in medical devices according to the ISO 10993–18:2020 standard. Fig. 10a presents the ATR-FTIR spectra obtained from all explanted surgical mesh samples. ATR-FTIR spectra of all explanted meshes show the appearance of pronounced carbonyl peaks (expected range: 1750–1500 cm^{-1}). ATR-FTIR spectra collected from control mesh (treated with protease Alcalase®) are presented in the supporting information Fig. SI2 and display no pronounced carbonyl peaks. Noteworthy, 180 days implanted mesh from both implantation sites showed a significant increase in carbonyl peaks compared to that of spectra of mesh implanted for 60 days. The appearance of carbonyl peaks at 1800 -1600 cm^{-1} have been long reported in relation to the oxidative degradation of PP (Imel et al., 2015; Jain et al., 2023; Farr et al., 2023a; Farr et al., 2023b).

Raman spectroscopy was performed to identify changes within the structural units of PP backbone structures. Raman spectroscopy is recommended in ISO 10993–18:2020 for the determination of the constituent structure of synthetic polymers. Fig. 10b shows the Raman spectra of all explanted samples recorded in the range 600–1600 cm^{-1}. It has been previously established that the 808, 841, 972, 995, 1168 cm^{-1} bands are related with the helical chain structure of PP (Tadokoro

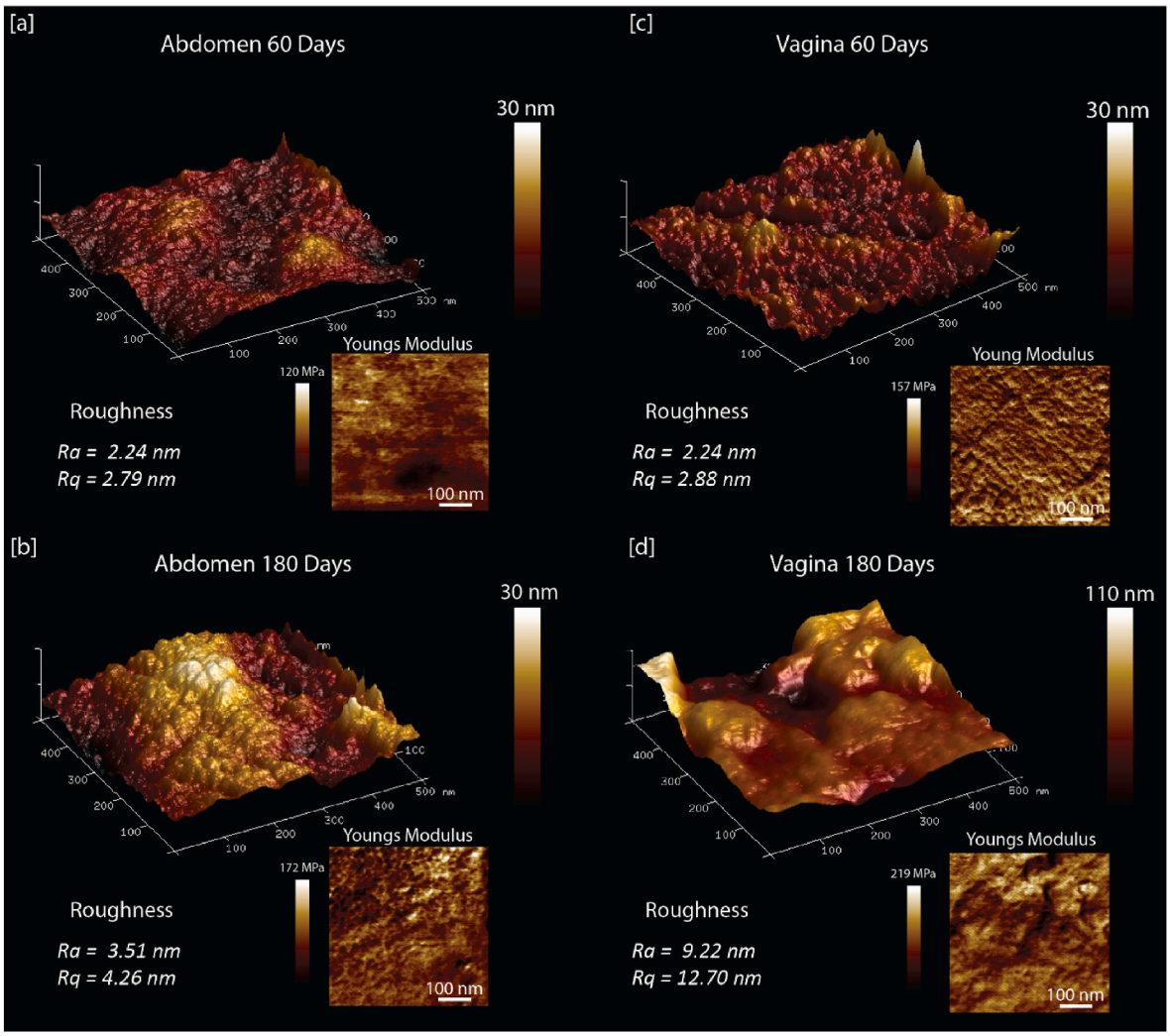

Fig. 8. 3D AFM surface topography micrographs and 2D AFM Young's modulus maps for explanted samples. Note that the height scale for [d] is 110 nm, compared with all other plots where height scale is 30 nm. AFM taken from control mesh (treated with protease Alcalase®) samples are provided in Fig. SI 2 of the supporting information.

et al., 1965). Variations within these band ratios, when viewed in terms of relative intensity normalised to PP reference band 972 cm^{-1}, reveal a notable helical structural change between explanted materials. One example of this variation can be seen when examining the band ratio of 808 and 841 cm^{-1} (Nielsen et al., 2002; Furukawa et al., 2006; Sundell et al., 1996). When comparing the intensity ratios of I841/I808, it is clear that the 180-day implantation period resulted in greater helical chain defects than were found in mesh implanted for just 60 days. This result further confirms a time dependent change in the bulk properties of the implanted PP consistent with oxidation of polymer chains.

4. Discussion

A summary of the key experimental findings of this study is presented in Fig. 11.

4.1. Impact summary

After decades of development, polypropylene mesh, having shown beneficial results for abdominal repair, was implanted in the pelvic floor of women suffering from SUI and POP. Clinical results of this intervention have unfortunately shown an unacceptable incidence of adverse complications in women. The assumption that a material which works well in one site in the body will therefore work well elsewhere has failed in this instance. As a consequence of the trauma suffered and the surgical difficulties of restoring the insertion site, the topic of mesh insertion has become extremely litigious and there has been relatively little critical work into why a material that works well in the abdomen causes such problems in the pelvic floor. With a better understanding of the host response to the mesh material the authors are hopeful that it will be possible to design materials which do not elicit inflammation and contraction of tissues resulting in distress to patients (as reviewed in Mangir et al. (2019)). The aim of this study was to undertake a detailed materials investigation of polypropylene mesh post implantation in the abdomen and vagina of sheep for 60 and 180 days. While this model doesn't replicate the mechanical tension seen in mesh devices used for patients with prolapse, it remains the most pertinent model available for evaluating how the biomaterial integrates and elicits a host response within the specific anatomical site. To this end, we have undertaken an extensive range of physical characterisation of explanted materials implanted in both sites of the body for different periods of time. It is important to note that this study only examined Restorelle polypropylene mesh. Different knit patterns, weights, densities, and additives within various types of polypropylene surgical mesh could impact the degradation of the resulting device. In brief the study provides a range of evidence (outlined in Fig. 11) that there is a time-dependent alteration in both the surface properties of the polypropylene fibres and in their bulk properties. In essence, the material becomes stiffer and

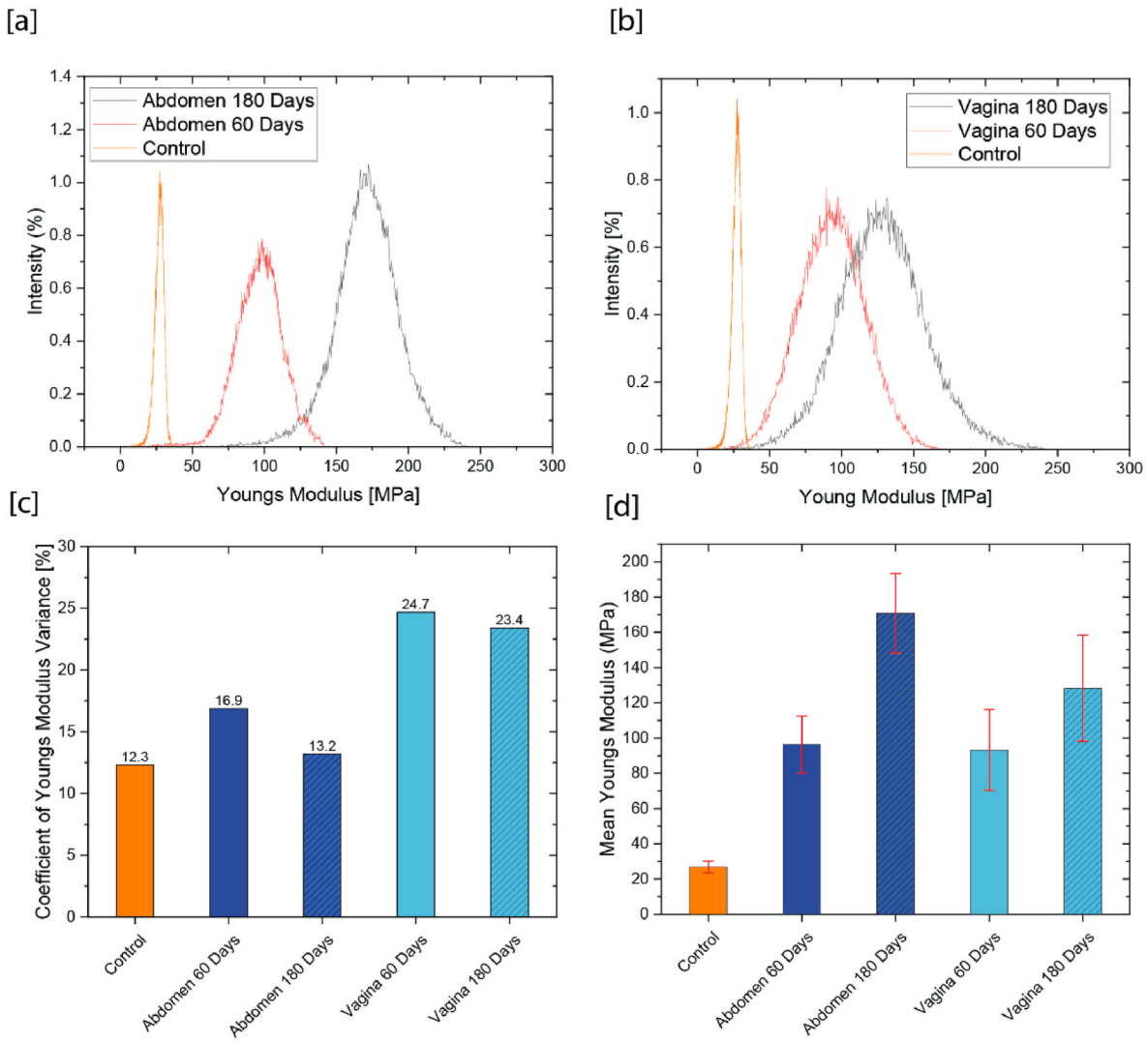

Fig. 9. [a] Young's modulus distribution histograms for explanted and control from the abdomen. [b] Young's modulus distribution histograms for explanted and control samples from the vagina. [c-d] graphs presenting the coefficient of variance [c] and mean [d] of the Young's Modulus obtained from all samples.

the oxidised surfaces shed small particles of oxidised material which migrate to the surrounding tissues. The results of this study highlight the challenges of selecting biomaterials suitable for medical interventions. Biomaterial selection is a complex and context dependent task. Selection of suitable biomaterials needs to be informed by knowledge of the anatomy and physiology of the tissues/organs which the material is being used to support. This raises a host of related questions:

What are the cellular aspects of the *in vivo* environment? What are the mechanical forces present within the *in vivo* environment? What is the expected duration of exposure of the biomaterial to the *in vivo* environment? How do the biomaterial properties change over time within the *in vivo* environment and what are the consequences of these biomaterial changes?

As evident, various biomaterial characteristics, such as mechanical-chemical properties, surface chemistry, surface topology, cell toxicity, chemical reactivity (whether inert or reactive), and the mechanical properties of biomaterials, all play a crucial role in determining their long-term compatibility with host tissues.

4.2. General discussion

In this study we have focused primarily on physical characterisation of the explanted PP mesh as it has been widely reported that a hostile inflammatory environment can lead to surface alterations in polymer derived-biomaterials (Clavé et al., 2010; Farr et al., 2023a; Anderson et al., 2008). It was expected that any PP *in vivo* degradation, as commonly observed in many plastics, would first occur at the polymer surface. The cryo-SEM images of explanted mesh from all groups showed tissue integration with what appears to be protein deposition around the mesh that was identifiable even after 60 days of implantation. The imaging conducted in this study reveals that environmental stress cracking (ESC) of explanted PP surgical mesh is more pronounced in the vagina compared to the abdomen. Findings from cryo-LVSEM, LV-SEM, and X-Ray tomography after tissue digestion suggest that the longer duration of implantation tends to overshadow the impact of the implantation site, particularly for the short durations considered in this study. This is not an unexpected finding as the model used to implant the mesh within the vagina does not mimic a urethral sling.

SEHI is a novel, highly sensitive surface technique that has been shown to be able to detect bonds on carbonaceous material surfaces (Farr et al., 2021b; Nohl et al., 2022). The application of SEHI showed that the surface chemistry of explanted PP fibres was not homogenous and that the peeling away of surface material was uncovering fresh regions of PP. For surgical mesh materials which had undergone 180 days implantation there was surface "barking" and an abundance of surface particles, identified in Figs. 5–7, which are cleaved away over time.

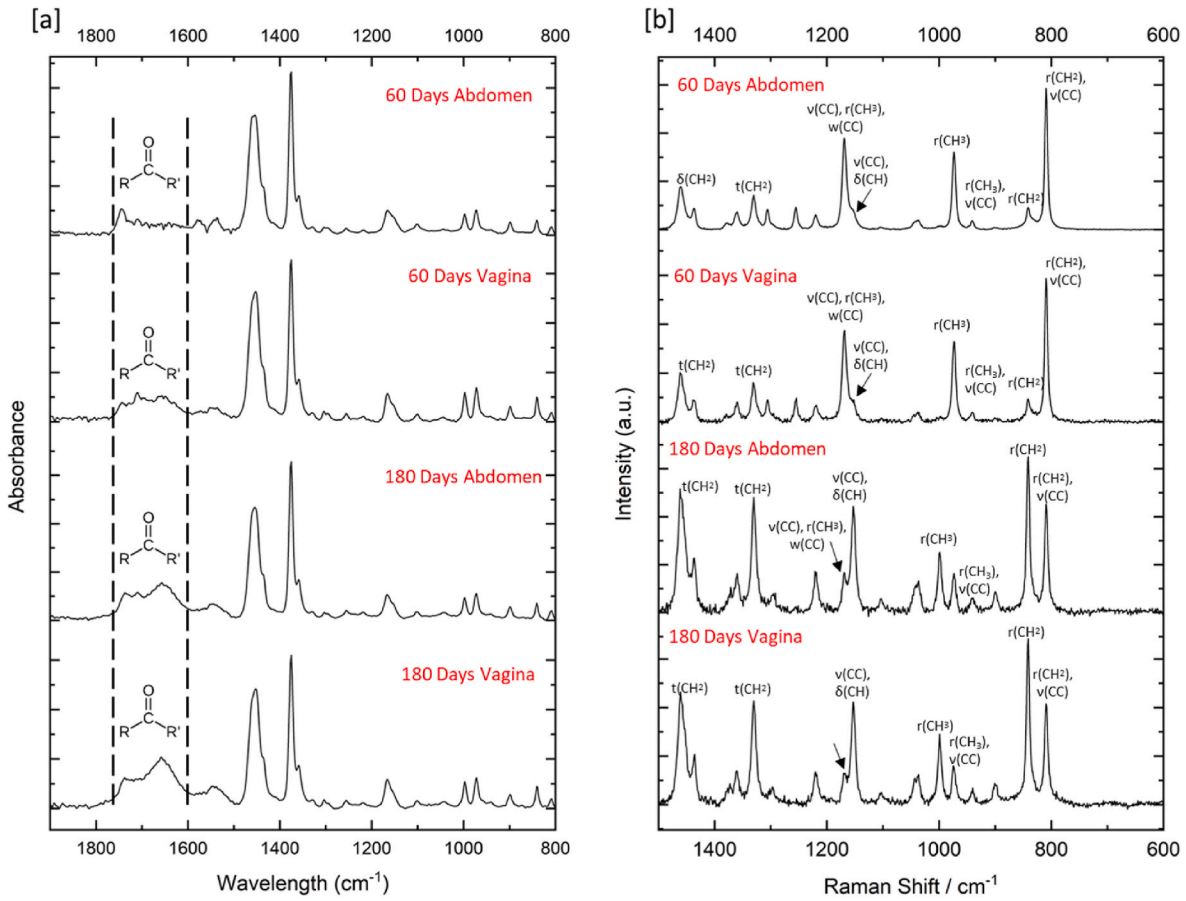

Fig. 10. [a] Attenuated total Reflectance-Fourier transform infrared spectroscopy (ATR-FTIR) spectra collected from explanted PP surgical mesh. Spectra of the explanted meshes show carbonyl peaks at 1800 -1600 cm−1 [b] Raman spectra of explanted PP surgical mesh.

These form the PP debris which was observed within the tissues identified by s-SNOM and pyrolysis gas chromatography mass spectrometry.

The identification of surface cracking and "barking" of PP surgical fibres after *in vivo* incorporation is not a novel finding. Studies have long shown PP fibres have a susceptibility to crack due to *in vivo* bio-instability (Iakovlev et al., 2017; Jongebloed et al., 1986). Clavé et al. (2010) characterised surgical mesh implants explanted from patients to evaluate the degradation characteristics of PP and found very similar cracking to that observed within Fig. 7 (Clavé et al., 2010). Similar to Clavé et al., and despite the shortened implantation duration applied in this study, our results also confirm the presence of surface degradation. Although studies have identified surface cracks and flaking this is the first study to identify PP debris resident within surrounding native tissue.

This study not only showed that the flaking of PP increased over time but also through the application of s-SNOM, to histology slides, we were able to identify that the resulting flakes were highly oxidised. This finding points to a mechanism previously stated (Farr et al., 2021a) that surface degradation, through oxidative stress, has the capacity to chemically etch the surface of PP fibres which leads to the formation of highly oxidised PP particles. How these particles are removed from the surface is likely due to mechanical shear being applied to the fibres.

An M1 macrophage phenotype has been associated with a chronic immune response and material rejection, leading to an increased formation of fibrotic tissue (Anderson et al., 2008). It is considered feasible that PP particles of micron scale size released into the *in vivo* mesh environment may instigate the inflammation of nearby cells which in turn release additional oxidising agents. This PP degradation/inflammation cycle would then have the potential to drive a positive feedback loop significantly increasing the expected immune response. Recent studies focused on the toxicology of PP material have shown that PP alone has the potential to trigger an increase in cell inflammation which in turn leads to an increase in PP fibre oxidation products. The clinical effect of PP particles *in vivo* is likely to be dependent on many factors, including: dose, surface chemistry, hydrophobicity, and ultimately particle size.

Previous studies have identified that the dynamic distention of PP mesh materials for just 3 days can cause irreversible modifications to the mechanical properties of bulk PP meshes (Roman et al., 2019). This study is the first to provide insights into the surface stiffness of PP mesh after *in vivo* implantation. The AFM data presented indicate that both the duration of implantation and the anatomical site impact surface roughness and local surface stiffness of explanted PP meshes. A longer implantation period of 180 days resulted in significant differences in both surface roughness and stiffness, with implantation in the vagina causing more pronounced surface alterations. These results are not surprising, given that mechanical energy can break and form chemical bonds, potentially affecting mechanical properties.

It is important to acknowledge that while our study focuses on surface stiffness changes, these observed surface alterations alone may not fully account for changes in bulk fibre mechanical properties. It is considered that the bulk mechanical properties of the mesh may also be influenced by geometric changes, such as shifts or sliding in the mesh knit pattern due to *in vivo* loading. These geometric changes, combined with surface modifications, may contribute to alterations in the mechanical properties of explanted PP mesh. However, it is worth noting that one limitation of this study is the lack of direct testing of the bulk mechanical properties of the material. The primary intention was to focus on surface changes using a comprehensive range of analytical techniques. Previous studies examining the effect of surface stiffness on

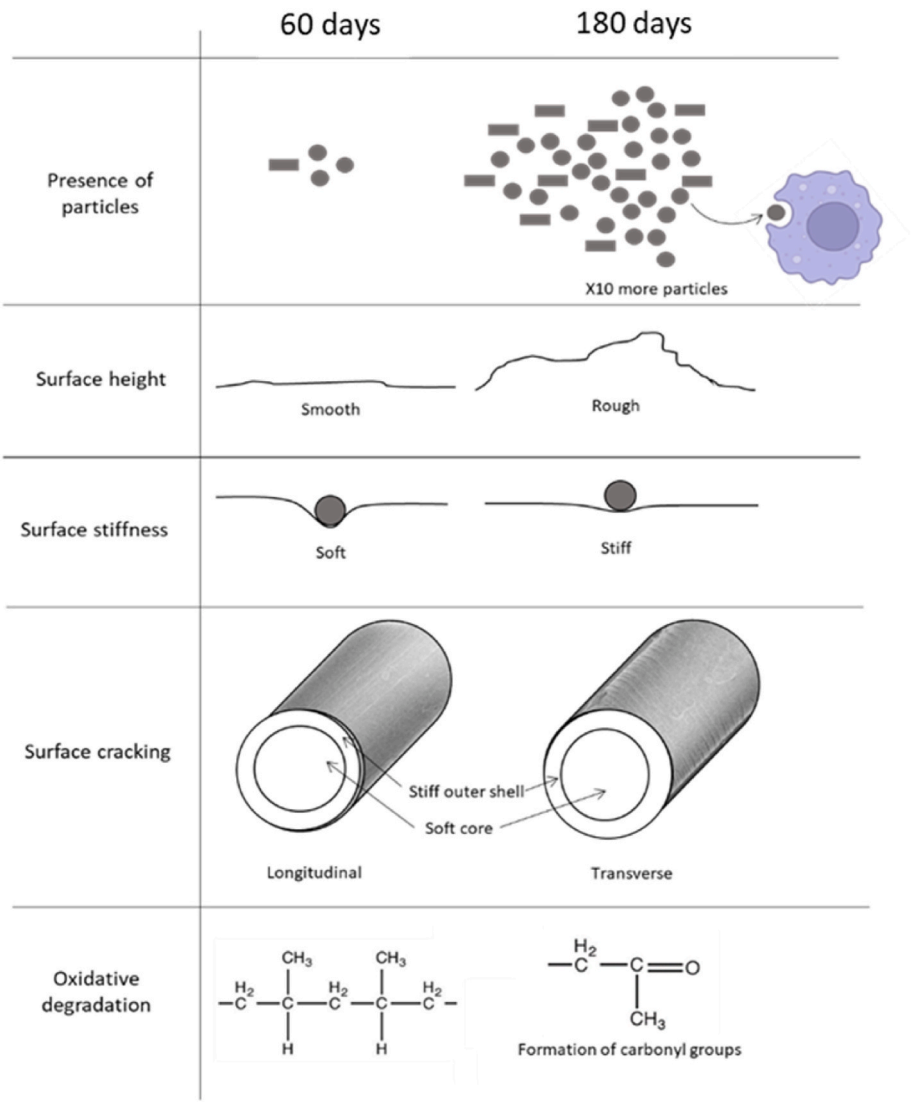

Fig. 11. Summary of the findings of this study.

bulk tensile strength suggest that prominent surface alterations are likely to impact bulk mechanical properties (Farr, 2023). In this instance, it is hypothesised that the longer duration of implantation and the different anatomical sites (specifically in the vagina, where greater variation in Young's modulus was identified) create conditions that favour the stiffening of PP fibres, potentially affecting both surface and bulk mechanical properties.

Our group have previously shown that the input of mechanical force can also affect the surface degradation of PP mesh, via oxidation (Farr et al., 2021a). As stated previously the mechanisms by which polypropylene degrades via oxidation have been extensively studied and documented. As has been seen within this study, it has been long observed that even a low level of oxidation can result in stress-cracking in semi-crystalline polyolefin, with embrittlement observed in PP (Celina et al., 1993; Farr, 2023; Pospisil et al., 1989). Results obtained from ATR-FTIR, Raman, s-SNOM and AFM show this is also the case for PP surgical mesh implanted in this model.

Studies have long documented the oxidation of PP, which includes the formation of a hydroperoxide prior to chain scission (Talley et al., 2017; Farr et al., 2023a), with subsequent formation of aldehydes, ketones, and carboxylic acids, with accompanying chain cleavage. ATR-FTIR data presented showed the appearance of peaks related to carboxyl groups, previously documented in relation to PP oxidative degradation, were more prominent in explanted mesh samples which had been incorporated for 180 days over 60 days and when implanted in the vagina over the abdomen. The degradation of PP mesh is proposed to be the result of the synergistic effects of corrosive chemicals such as reactive oxygen species (ROS) produced by inflammatory cells and tensile stress in the mesh fibres *in vivo*. The Raman spectra obtained were in agreement with ATR-FTIR findings. The longer implantation time and the chosen site of the vagina, instead of the abdomen, resulted in greater helical polymer chain defects. An oxidation mechanism has been proposed for PP degradation *in vivo* with the consequences of PP oxidation on fibre properties have been considered and studied extensively, to include fibre cracking/crazing, flaking, molecular alterations, loss of elasticity, and embrittlement.

5. Conclusions

This study presents data illustrating a correlation between extended implantation periods of PP mesh and a progressive escalation in oxidative and surface degradation. Notably, the prevalence of particles exhibited a significant surge between the 60 and 180-day milestones. These particles were examined through innovative microscopy techniques, with quantitative analysis carried out using Py-GC-MS. Employing histology and scattering-type s-SNOM, particles were

identified as being embedded within the sheep tissue and displayed an oxidised surface. The study also documented the emergence of small transverse surface cracks after 60 days of implantation, evolving into deeper and wider fissures by the 180-day mark. Data obtained from AFM further underscored that the longer the mesh remained implanted, the greater the increase in fibre surface stiffness and variations in surface height. This comprehensive assessment sheds light on the evolving structural changes and material properties of PP surgical mesh *in vivo* over extended durations, providing valuable insights into its long-term performance and implications for biomedical applications.

Funding

This work was supported by Engineering and Physical Sciences Research Council (EPSRC) [N.T.H.F grant: EP/T517835/1, N.T.H.F, D. A.G and C.R thank the Diamond Light Source for beamtime (proposal MG33034-1). N.T.H.F and C.R grant: EP/V012126/1]; Medical Research Council (MRC) through the Confidence in Concept scheme [N.T.H.F, C. R, S.R, and S.M]; The Luff Foundation [V.W.]. A.J.K. and A.I.T. thank the support of EPSRC grant EP/V007696/1. C. Rauert's salary is funded by the Minderoo Foundation, an independent not for profit philanthropic organisation. The Queensland Alliance for Environmental Health Sciences, The University of Queensland, gratefully acknowledges the financial support of Queensland Health.

CRediT authorship contribution statement

Nicholas T.H. Farr: Writing – review & editing, Writing – original draft, Visualization, Validation, Supervision, Resources, Project administration, Methodology, Investigation, Funding acquisition, Formal analysis, Data curation, Conceptualization. **David A. Gregory:** Writing – review & editing, Visualization, Methodology, Formal analysis, Data curation. **Victoria L. Workman:** Writing – review & editing, Writing – original draft, Project administration, Methodology, Investigation, Formal analysis. **Cassandra Rauert:** Writing – review & editing, Methodology, Investigation, Formal analysis, Data curation. **Sabiniano Roman:** Writing – review & editing, Resources, Project administration, Investigation. **Alexander J. Knight:** Writing – review & editing, Writing – original draft, Methodology, Investigation, Formal analysis, Data curation. **Anthony J. Bullock:** Writing – review & editing, Project administration, Methodology. **Alexander I. Tartakovskii:** Supervision, Resources, Project administration, Methodology, Funding acquisition. **Kevin V. Thomas:** Writing – review & editing, Supervision, Resources, Project administration, Methodology, Investigation. **Christopher R. Chapple:** Writing – review & editing, Supervision, Project administration, Investigation, Funding acquisition. **Jan Deprest:** Resources, Project administration, Methodology, Investigation, Funding acquisition, Formal analysis, Data curation. **Sheila MacNeil:** Writing – review & editing, Writing – original draft, Supervision, Resources, Project administration, Methodology, Investigation. **Cornelia Rodenburg:** Writing – review & editing, Writing – original draft, Visualization, Supervision, Resources, Project administration, Investigation.

Declaration of competing interest

The authors declare the following financial interests/personal relationships which may be considered as potential competing interests: N.T.H.F has provided expert testimony for lawsuits concerning surgical mesh. This testimony was provided subsequent to the analysis and submission of this manuscript. J.D research program has previously received funding from Johnson & Johnson, Blasingame, Burch, Garrard and Ashley (Atlanta, GA), Clayton Utz (Sydney, Australia).

Data availability

Data will be made available on request.

Acknowledgments

N.T.H.F acknowledges the Sorby Centre for Electron Microscopy at the University of Sheffield for allowing electron microscopy and analysis to be performed.

Appendix A. Supplementary data

Supplementary data to this article can be found online at https://doi.org/10.1016/j.jmbbm.2024.106722.

References

Abed, H., et al., 2011. Incidence and management of graft erosion, wound granulation, and dyspareunia following vaginal prolapse repair with graft materials: a systematic review. Int Urogynecol J 22 (7), 789–798.
Anderson, J.M., Rodriguez, A., Chang, D.T., 2008. Foreign body reaction to biomaterials. Semin. Immunol. 20 (2), 86–100.
Celina, M., George, G.A., 1993. A heterogeneous model for the thermal oxidation of solid polypropylene from chemiluminescence analysis. Polym. Degrad. Stabil. 40 (3), 323–335.
Clavé, A., et al., 2010. Polypropylene as a reinforcement in pelvic surgery is not inert: comparative analysis of 100 explants. Int Urogynecol J 21 (3), 261–270.
Deplaine, H., et al., 2013. Biomimetic hydroxyapatite coating on pore walls improves osteointegration of poly(L-lactic acid) scaffolds. J. Biomed. Mater. Res. B Appl. Biomater. 101 (1), 173–186.
Fakhrullina, G., et al., 2017. Nanoscale imaging and characterization of Caenorhabditis elegans epicuticle using atomic force microscopy. Nanomed. Nanotechnol. Biol. Med. 13 (2), 483–491.
Farr, N.T.H., 2023. Regulating the formation and extent of crazing through the application of argon plasma surface functionalisation. Polym. Test. 128, 108244.
Farr, N.T.H., et al., 2021a. A novel characterisation approach to reveal the mechano–chemical effects of oxidation and dynamic distension on polypropylene surgical mesh. RSC Adv. 11 (55), 34710–34723.
Farr, N., et al., 2021b. Understanding surface modifications induced via argon plasma treatment through secondary electron hyperspectral imaging. Adv. Sci. 8 (4), 2003762.
Farr, N.T.H., Klosterhalfen, B., Noé, G.K., 2023a. Characterization in respect to degradation of titanium-coated polypropylene surgical mesh explanted from humans. J. Biomed. Mater. Res. B Appl. Biomater. 111 (5), 1142–1152.
Farr, N.T.H., et al., 2023b. Characterization and quantification of oxidative stress induced particle debris from polypropylene surgical mesh. Nano Select 4 (6), 395–407.
Farr, N., et al., 2024. Uncovering the relationship between macrophages and polypropylene surgical mesh. Biomater. Adv. (in press).
Furukawa, T., et al., 2006. Molecular structure, crystallinity and morphology of polyethylene/polypropylene blends studied by Raman mapping, scanning electron microscopy, wide angle X-ray diffraction, and differential scanning calorimetry. Polym. J. 38 (11), 1127–1136.
Hympánová, L., et al., 2020. Assessment of electrospun and ultra-lightweight polypropylene meshes in the sheep model for vaginal surgery. European Urology Focus 6 (1), 190–198.
Iakovlev, V.V., Guelcher, S.A., Bendavid, R., 2017. Degradation of polypropylene in vivo: a microscopic analysis of meshes explanted from patients. J. Biomed. Mater. Res. B Appl. Biomater. 105 (2), 237–248.
Imel, A., et al., 2015. In vivo oxidative degradation of polypropylene pelvic mesh. Biomaterials 73, 131–141.
Jain, T., et al., 2023. Accelerated in vitro oxidative degradation testing of polypropylene surgical mesh. J. Biomed. Mater. Res. B Appl. Biomater. 111 (12), 2064–2076.
Jongebloed, W.L., Worst, J.F., 1986. Degradation of polypropylene in the human eye: a SEM-study. Doc. Ophthalmol. 64 (1), 143–152.
Kroese, L.F., et al., 2017. Long term results of open complex abdominal wall hernia repair with self-gripping mesh: a retrospective cohort study. Int. J. Surg. 44, 255–259.
Mangir, N., et al., 2019. Landmarks in vaginal mesh development: polypropylene mesh for treatment of SUI and POP. Nat. Rev. Urol. 16 (11), 675–689.
Milsom, I., Gyhagen, M., 2014. The epidemiology, natural history and prevention of pelvic floor disorders. In: The Global Library of Women's Medicine.
Nielsen, A.S., Batchelder, D.N., Pyrz, R., 2002. Estimation of crystallinity of isotactic polypropylene using Raman spectroscopy. Polymer 43 (9), 2671–2676.
Nohl, J.F., et al., 2022. Low-voltage SEM of air-sensitive powders: from sample preparation to micro/nano analysis with secondary electron hyperspectral imaging. Micron 156, 103234.
Pospisil, J., Klemchuk, P.P., 1989. In: Oxidation Inhibition in Organic Materials. CRC Press, p. 384.
Roman, S., et al., 2019. Use of a simple in vitro fatigue test to assess materials used in the surgical treatment of stress urinary incontinence and pelvic organ prolapse. Neurourol. Urodyn. 38 (1), 107–115.
Sundell, T., Fagerholm, H., Crozier, H., 1996. Isotacticity determination of polypropylene using FT-Raman spectroscopy. Polymer 37 (15), 3227–3231.

Tadokoro, H., et al., 1965. Normal vibrations of the polymer molecules of helical conformation. V. Isotactic polypropylene and its deuteroderivatives. J. Chem. Phys. 42, 1432–1449.
Talley, A.D., et al., 2017. Oxidation and degradation of polypropylene transvaginal mesh. J. Biomater. Sci. Polym. Ed. 28 (5), 444–458.
Taylor, D., 2018. The failure of polypropylene surgical mesh in vivo. J. Mech. Behav. Biomed. Mater. 88, 370–376.
Thames, S.F., White, J.B., Ong, K.L., 2017. The myth: in vivo degradation of polypropylene-based meshes. Int Urogynecol J 28 (2), 285–297.
Ulmsten, U., et al., 1996. An ambulatory surgical procedure under local anesthesia for treatment of female urinary incontinence. Int. UrogynEcol. J. Pelvic Floor Dysfunct. 7 (2), 81–85. ; discussion 85-6.
Usher, F.C., 1962. Hernia repair with Marlex mesh. An analysis of 541 cases. Arch. Surg. 84, 325–328.
Usher, F.C., Ochsner, J., Tuttle Jr., L.L., 1958. Use of marlex mesh in the repair of incisional hernias. Am. Surg. 24 (12), 969–974.
Wang, H., et al., 2021. Degradation resistance of PVDF mesh in vivo in comparison to PP mesh. J. Mech. Behav. Biomed. Mater. 119, 104490.